International Journal of Heat and Technology
Vol. 40, No. 5, October, 2022, pp. 1133-1140
Journal homepage: http://iieta.org/journals/ijht

Electrical Production Effect on the Planar Solid Oxide Fuel Cell Overheating

Youcef Sahli[1], Houcine Moungar[1*], Mohammed Benhammou[1], Bariza Zitouni[2], Hocine Ben-Moussa[3]

[1] Unité de Recherche en Energies Renouvelables en Milieu Saharien, URERMS, Centre de Développement des Energies Renouvelables CDER, Adrar 01000, Algeria
[2] Institut des Sciences Vétérinaires et des Sciences Agronomiques, Université de Batna 1, Batna 05000, Algeria
[3] Département de Mécanique, Faculté de Technologie, Université de Batna 2, Batna 05000, Algeria

Corresponding Author Email: h.moungar@urerms.dz

https://doi.org/10.18280/ijht.400503

Received: 25 September 2019
Accepted: 16 August 2022

Keywords:
P-SOFC, heat, current density, overheating

ABSTRACT

In this work, a steady-state three-dimensional model is employed to investigate the heat transfer phenomena in a Planar Solid Oxide Fuel Cell (P-SOFC) and determine the current density impact on the overheating of this fuel cell type. The thermoelectric characteristics of various components of the P-SOFC are provided from the standard materials: Ni-YSZ for the anode, YSZ for the electrolyte, La1-xSrxMnO$_3$ for the cathode, and LaCrO$_3$ for the interconnectors. The partial differential equations governing the heat transfer phenomena in the different cell parts are modelled using the finite difference method in a three-dimensional environment. A program in FORTRAN language is locally developed for solving simultaneously the discretized heat conduction equation. The interest of this work is focused on determining the temperature profiles, fields, and distributions as well as evaluating and analysing the heat created by the current densities produced by the cell itself. The obtained results' analysis shows that for the considered geometric configuration, the P-SOFC components' heating is found to be proportional to the electric energy production.

1. INTRODUCTION

In the last few decades, the growth in energy demand and environmental protection problems required finding new energy sources more productive and less polluting. Fuel cells appear as a tool of clean energy production in the future, which use hydrogen as fuel. They convert chemical energy into electrical energy. They are generally classified according to their operating temperature. The high operating temperature of SOFC causes a very large heat exchange between their various components, in which the heat is produced in several ways.

Owing to the complexity due to multiple phenomena taking place when operating these fuel cells makes it difficult to evaluate separately these phenomena in the experiment. Alternatively, the research laboratory developed numerical simulation programs can better predict and assess simultaneously and individually the behavior of happening phenomena. In this context, several studies concerning Solid Oxide Fuel cells have been addressed in the literature. Inui et al. [1] have studied the influence of the hydrogen and carbon monoxide mixture in the fuel on the P-SOFC performance in a three-dimensional environment. Sun and Ou [2] have investigated and evaluated the influence of channel designs on the power density in a single P-SOFC unit using an unsteady three-dimensional model by disregarding radiation heat exchanges. They have compared also the results of 3 different oxidant compositions; 100% O_2, 50% N_2 / 50% O_2 and air. Similarly, Danilov and Tade [3] have used and applied an unsteady three-dimensional model to investigate a SOFC stack, which consists of 29 parallel cells, the model includes fluid dynamics, electrochemistry, mass and heat transfers by considering only two modes of them: conductive and convective. Heat energy production is caused by the activation of chemical reactions and ohmic losses. In addition, the results are obtained by resolving the equations relating to the involved phenomena using the most used commercial code 'FLUENT'. They have finally confirmed that their proposed model is useful for optimizing the SOFC design. Moreover, Chaisantikulwat et al. [4] have presented an unsteady three-dimensional model for a P-SOFC, which provides the polarization curves, the molar fraction, gas speeds, temperatures, species concentrations, and current distributions. Yang et al. [5] have employed a steady-state three-dimensional tool, to simulate the impact of several parameters in P-SOFCs. They have neglected the radiative heat transfer and taken into account that the heat is generated according to several mechanisms, namely the heat sources due to the electrochemical reactions, activation overvoltage, and ohmic. The elaborated numerical tool is then used to simulate a set of parameters such as temperature, species, current densities, etc. Ho et al. [6] have examined the influence of air inlet conditions, chemical species, and current density distributions for the counter and co-flow configurations. The unsteady three-dimensional model consisted of the coupling of different physical phenomena such as fluid dynamics, electric charge transport as well as mass and heat transfers. In their analysis carried out using Star-CD commercial code, the radiative heat transfer and all heat source types, except the chemical source are neglected. They have shown that the results obtained with the counter-flow configuration are better compared to the co-flow configuration. Khaleel et al. [7] have elaborated a simulation tool for P-SOFCs using the MARC analysis code,

with an electrochemical module developed by the authors to calculate the current distribution, heat production, and fuel and oxidant species concentrations. Wang et al. [8] have conducted a steady-state, three-dimensional, numerical simulation tool for SOFCs study based on the finite volume method. They have analyzed the temperature distributions, gas molar concentrations, current density, and the potential for both flowing modes: counter and co-flow.

Andreassi et al. [9] have studied and analyzed the species diffusion within electrodes, gases flow within the channels, the current density within solid and porous elements, and temperature distributions within the volume according to a circular stage of a P-SOFC with a supported anode using FEMLAB code. They have developed a steady-state three-dimensional model to account for the fluid dynamic, mass and electrical charge transfers, electrochemical reactions, and heat transfer by conduction and convection. In this study, radiative heat transfers are ignored and only the ohmic and activation losses are recognized as heat sources. Peksen [10, 11] has presented a three-dimensional thermo-mechanical study of a small stage of six P-SOFC cells to locate the critical areas. The model includes the electrochemical, heat transfer, and fluid dynamics in the cell channels, the heat production is considered produced by only the Ohmic loss. The investigation was performed using two commercial codes: ANSYS for mechanical structure and FLUENT for others studied parameters. Peksen et al. [12] have presented a three-dimensional thermo-mechanical investigation of a complete SOFC stack (stages, wire-mesh, metal frame, and sealing) to study the thermo-mechanical stress during heating, operating, and off provided by the CSM code. Nakajo et al. [13, 14] have presented a three-dimensional analysis of the mechanical reliability and durability of a P-SOFC with supported anode and parallel channels for two configurations (counter- and co-flow) using ABAQUS and gPROMS. A steady-state three-dimensional model is employed using FLUENT and ANSYS commercial codes to study the thermal behavior and stress in a P-SOFC and its sealing gasket [15]. Hawkes et al. [16] have proposed a new model to study the influence of several parameters on the performance of a SOFC stack of sixty cells with cross-flow, which represents a quarter of the I.L.S module of Ceramatec, using FLUENT commercial code. Lee and Hong [17] have presented an unsteady three-dimensional simulation of the P-SOFC consisting of five cells and an air preheat chamber using ADINA-CFD. Yan et al. [18] have examined and evaluated the exterior design of a small P-SOFC stack of three stages of monolithic channels configuration and a cross-flow using ANSYS commercial code.

Based on our previous works on the PEMFC and SOFC technology [19-31] as well as the consulted literature [1-18], where this subject has received considerable attention in the literature, but the electrical production effect on SOFC overheating is not yet apparent and undetailed. This present work focuses on obtaining and analyzing the profiles and distributions of the temperature of a single cell P-SOFC, with the same element hart dimensions, according to a steady-state three-dimensional model, when, in the conducted investigation, only the ohmic loss is considered as the heat source to study and determine the current density impact on the P-SOFC heating. Joule's effect is considered in all P-SOFC components; namely, anode, cathode, electrolyte, and both anodic and cathodic interconnectors to study the electrical production effect on SOFC overheating. A FORTRAN code is developed locally based on the proposed model, which is discretized using the finite difference method, to accomplish this study.

Generally, the heat produced inside the P-SOFC components is uneven and generates non-uniform distributions of temperature due to the variety of construction materials and the role of each component as well as their operating conditions. In this present study, several investigations, using the elaborated code, are conducted to localize and determine the hottest zones inside the P-SOFC, for the imposed current densities of 4000, 6000, 12000, and 200000 A/m^2 and an inlet gas temperature in both channels of 1023 K, to know the impact of the produced current density on the temperature filed of the P-SOFC.

2. MATHEMATIC MODEL

The computational domain considered in this study is limited to a P-SOFC single cell that consists of two gas flow channels, an anode, a cathode, an electrolyte, and two interconnectors (Figure 1).

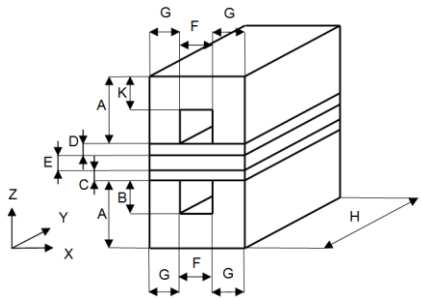

Element	Size (μm)
A	3000
B	2000
C	500
D	500
E	500
F	2000
G	1000
H	30000
K	1000

Figure 1. P-SOFC single cell dimension

Radiative heat transfers between the various cell components are neglected [2, 5, 6, 8, 9]. Energy is transmitted by convection and conduction within the anodic and cathodic channels [2-9]. At channels, gas velocities are considered low, so the convective term is negligible [22, 28]. Thereby, the energy is transported only by conduction in the solid and porous parts of the cell [22, 28], and in addition, only the ohmic overpotential is considered as an internal heat source [10-11, 28].

On account of the above assumptions, the equation of energy conservation is given by the following equation:

When considering Joule's effect, this equation is rewritten as:

$$\frac{\partial}{\partial x}\left(\lambda\frac{\partial T}{\partial x}\right)+\frac{\partial}{\partial y}\left(\lambda\frac{\partial T}{\partial y}\right)+\frac{\partial}{\partial z}\left(\lambda\frac{\partial T}{\partial z}\right)=0 \quad (1)$$

When considering Joule's effect, this equation is rewritten as follow.

$$\frac{\partial}{\partial x}\left(\lambda\frac{\partial T}{\partial x}\right)+\frac{\partial}{\partial y}\left(\lambda\frac{\partial T}{\partial y}\right)+\frac{\partial}{\partial z}\left(\lambda\frac{\partial T}{\partial z}\right)+S_j=0 \quad (2)$$

$$S_j=\frac{i^2}{\sigma_j} \quad (3)$$

where, j: anode, cathode, electrolyte, or interconnector.

The electrical conductivity of each P-SOFC component is given in Table 1.

Table 1. Electrical conductivity of P-SOFC components

Components	Electrical conductivity σ	References
Electrolyte	$\sigma_{ele} = 3.34 \times 10^4 exp\left(\frac{-10300}{T}\right)$	[9, 28, 32-40]
Cathode	$\sigma_{cat} = \frac{4.2\times10^7}{T} exp\left(\frac{-1200}{T}\right)$	[33-35, 37, 39]
Anode	$\sigma_{an} = \frac{9.5\times10^7}{T} exp\left(\frac{-1150}{T}\right)$	[9, 28, 33-40]
Interconnector	$\sigma_{in} = 9.3 \times 10^6 exp\left(\frac{-1100}{T}\right)$	[33, 35, 39, 41]

Table 2. Boundary conditions

Components	OX axis		OY axis		OZ axis	
	(0,y,z)	(L_x,y,z)	(x,0,z)	(x,L_y,z)	(x,y,0)	(x,y,L_z)
Electrolyte	$\frac{\partial\Phi}{\partial x}=0$	$\frac{\partial\Phi}{\partial x}=0$	$\frac{\partial\Phi}{\partial y}=0$	$\frac{\partial\Phi}{\partial y}=0$	$\frac{\partial\Phi}{\partial z}=0$	$\frac{\partial\Phi}{\partial z}=0$
Cathode	$\frac{\partial\Phi}{\partial x}=0$	$\frac{\partial\Phi}{\partial x}=0$	$\frac{\partial\Phi}{\partial y}=0$	$\frac{\partial\Phi}{\partial y}=0$	$\frac{\partial\Phi}{\partial z}=0$	$\frac{\partial\Phi}{\partial z}=0$
Anode	$\frac{\partial\Phi}{\partial x}=0$	$\frac{\partial\Phi}{\partial x}=0$	$\frac{\partial\Phi}{\partial y}=0$	$\frac{\partial\Phi}{\partial y}=0$	$\frac{\partial\Phi}{\partial z}=0$	$\frac{\partial\Phi}{\partial z}=0$
Interconnectors	$\frac{\partial\Phi}{\partial x}=0$	$\frac{\partial\Phi}{\partial x}=0$	$\frac{\partial\Phi}{\partial y}=0$	$\frac{\partial\Phi}{\partial y}=0$	$\frac{\partial\Phi}{\partial z}=0$	$\frac{\partial\Phi}{\partial z}=0$
Anode channel	$\frac{\partial\Phi}{\partial x}=0$	$\frac{\partial\Phi}{\partial x}=0$	$T = T_{H_2}$	$\frac{\partial\Phi}{\partial y}=0$	$\frac{\partial\Phi}{\partial z}=0$	$\frac{\partial\Phi}{\partial z}=0$
Cathode channel	$\frac{\partial\Phi}{\partial x}=0$	$\frac{\partial\Phi}{\partial x}=0$	$T = T_{air}$	$\frac{\partial\Phi}{\partial y}=0$	$\frac{\partial\Phi}{\partial z}=0$	$\frac{\partial\Phi}{\partial z}=0$

Table 3. Thermal conductivities of the different components

Components	Thermal conductivity λ(Wm^{-1}K^{-1})	Materials	References
Anode	5.84	Ni-YSZ	[1, 28, 42-44]
Cathode	4	$La_{1-x}Sr_xMnO_3$	[28, 42, 45-48]
Electrolyte	2.16	YSZ	[1, 28, 42-44]
Interconnector	6	$LaCrO_3$	[28, 49, 50]

At all external surfaces in all directions, the boundary conditions considered are of Neumann type, except at both channels inlet, where we take a constant temperature with Dirichlet conditions. The boundary conditions are shown in Figure 2 and Table 2.

The electrical and thermal conductivities of P-SOFC components are provided by the standard materials: Ni-YSZ, YSZ, $La_{1-x}Sr_xMnO_3$, and $LaCoO_3$ for the anode, electrolyte, cathode, and interconnectors (Table 3).

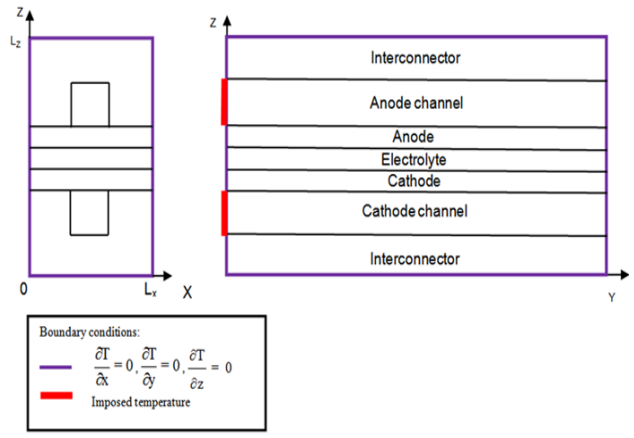

Figure 2. P-SOFC elementary cell boundary conditions

3. RESULTS AND DISCUSSIONS

Based on the presented model in the previous section, a FORTRAN language program has been realized locally to investigate the produced electrical effect on the overheating of P-SOFC heart elements. The cell heart element thicknesses are given by the same dimension of 500 µm. The inlet gas temperatures in both channels are the same, they are defined by a value equal to 1023 K [4, 32]. The mesh independence analysis between five numbers of cells was realized when cell number 115661 was considered (Figure 3.a). The comparison between the numerical results of this work and the numerical results of Sahli et al. [30] is shown in Figure 3.b.

At an imposed current density equal to 4000 A/m^2, Figure 4 shows that the maximum temperature values are located at the inlet of anodic and cathodic channels, they are identical to those of gases at the cell inlet (1023 K).

The lowest temperature values are around 1020 K. They are found in the cell outlet at the bottom part (interconnect lower part of the cathodic side, furthest from electrolyte). It should be noted that the temperature decreases from the inlet to the outlet of the cell due to the material thermal resistivity of the various components, which means that the joule's effect is not sufficiently important to increase the P-SOFC temperature values.

Cells operating at a current density value greater than 4000 A/m^2 have almost the same temperature field with an increase of the temperature values from the inlet to the cell outlet, which means that the maximum temperature value is situated at the stack outlet (Figures 5-7). Therefore, the minimum temperatures are those of the inlet gas (1023 K). This implies a heat generation case, wherein the produced thermal energy amount due to the ohmic loss is greater than those consumed due to the thermal resistivity of cell construction materials and this proves that in this last case, Joule's effect is found to have significant contributions. It is also demonstrated that the highest temperature is reported by the highest current density (20000 A/m^2); its value is estimated at 1225 K (Figure 7).

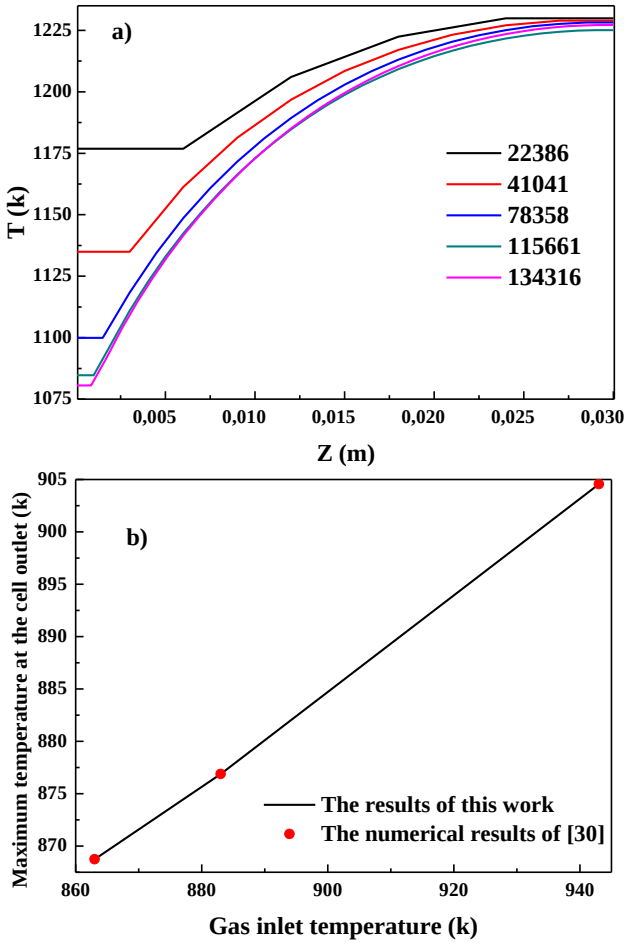

Figure 3. Mesh independence and validation: a) Mesh independence analysis, b) Comparison between the numerical results of this work and the numerical results [30]

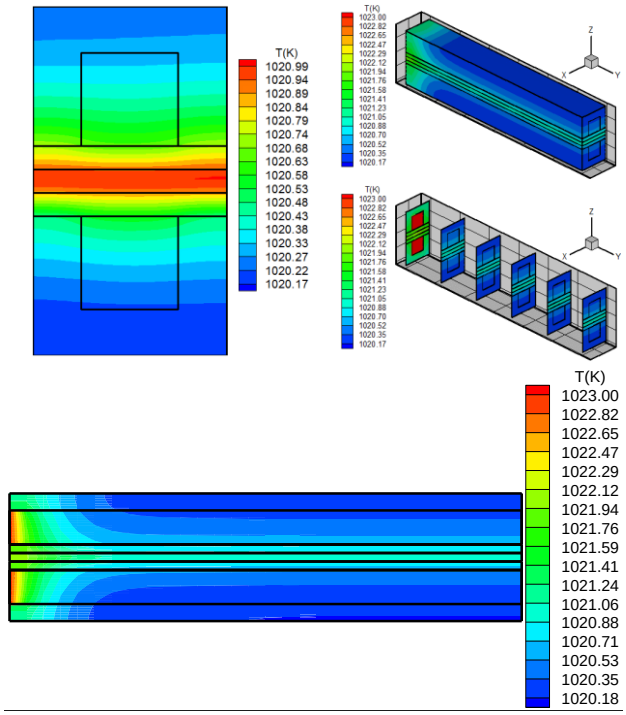

Figure 4. P-SOFC temperature field according to an imposed current density value of 4000 A/m^2

The maximum temperature values obtained according to the current densities are shown in Table 4. As can be seen, the maximum temperatures are located in the cell outlet, exactly at the anode/electrolyte interface (electrolyte upper part and bottom of the anode) (Figures 5-7).

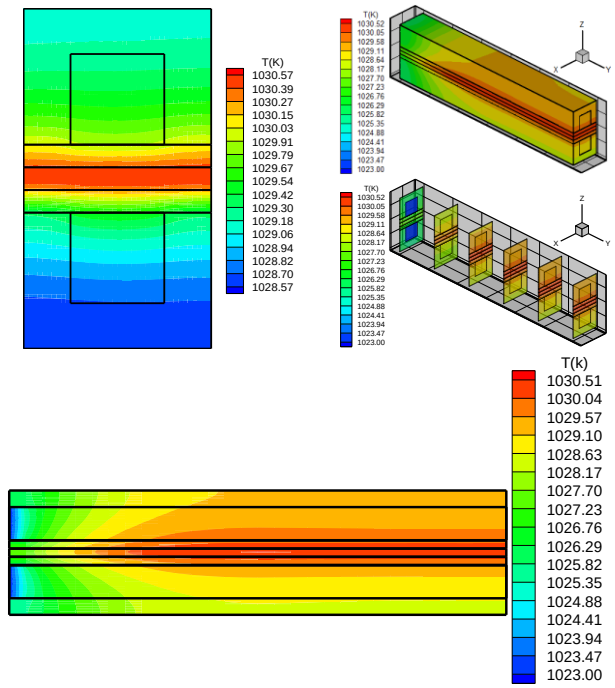

Figure 5. P-SOFC temperature field according to an imposed current density value of 6000 A/m^2

Table 4. Maximal temperature values

Current density (A/m^2)	T_{max} (K)
4000	1023.00 (Figure 4)
6000	1030.52 (Figure 5)
12000	1130.62 (Figure 6)
20000	1225.11 (Figure 7)

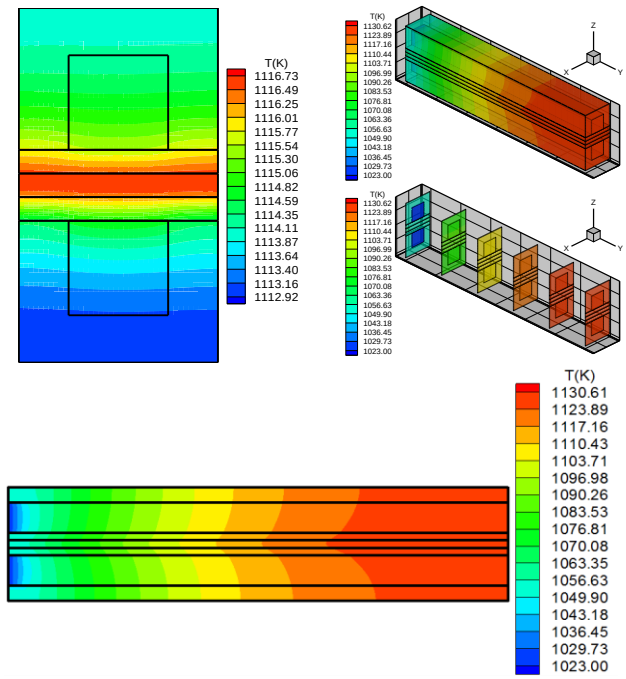

Figure 6. P-SOFC temperature field according to an imposed current density value of 12000 A/m^2

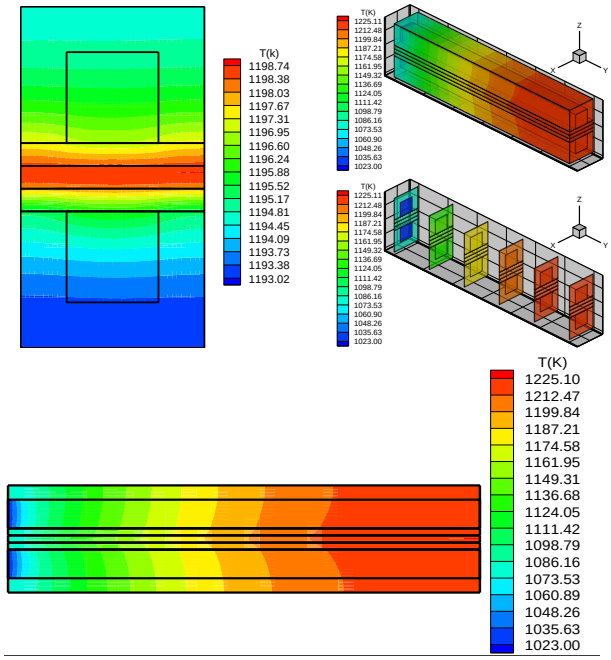

Figure 7. P-SOFC temperature field according to an imposed current density value of 20000 A/m^2

Furthermore, the interconnector top part (anodic part) is relatively hotter than the interconnector lower part (cathodic part) for cells at a current density greater than 4000 A/m^2 (Figures 5-7). Besides, another observation that should be highlighted, is the existence of a field symmetry to the (OZ) axis at x = 0.5.x$_{max}$ position in all studied cases (Figures 4, 5, 6, and 7).

For each current density at the cell outlet in the positions x = 0 and x = 0.5.x$_{max}$ the variations and distributions of the temperature along the (OZ) axis are shown in Figure 8.

The range of the temperature values variation on the (OZ) axis is about 5 K at the cell having a current density of 20000 A/m^2. The temperature variation at the cell exits on the (OZ) axis in the middle of the (OX) direction and the left side of the P-SOFC for a current density of 12000 A/m^2 is about 4 K. The interval between the extreme temperature values corresponding to a current density of 6000 A/m^2 at the cell outlet on the (OZ) axis at the cell middle and the left end is 2 K. Finally, the difference between the maximum and minimum temperature values on the same axis (OZ) and same positions (x = 0 and x = 0.5.x$_{max}$) at the outlet of the P-SOFC working at a current density 4000 A/m^2 is 1 K (Figure 8).

The maximal temperature values are located at a middle position on the (OX) axis; they are spotted in the same spatial coordinates in the 4 cases at a distance of 15 µm from the anode at the same height to the right and left extremity of the cell (Figure 8).

For each current density value, at the stack output in the middle of each component of the cell heart, the variations of the temperature along the (OX) axis are shown in Figure. 9. Because of the physical and geometric symmetries on the (OZ) axis at (x = 0.5.x$_{max}$), the curves are displayed from the left edge to the middle of the cell.

At the cell exit and in the middle of cell principal components, the maximum variation of the temperature values is registered at the cathode (0.4 K) at a current density equivalent to 20000 A/m^2 and it is about 0.2, 0.05, and 0.1 K for the current densities 12000, 6000, and 4000 A/m^2, respectively (Figure 9).

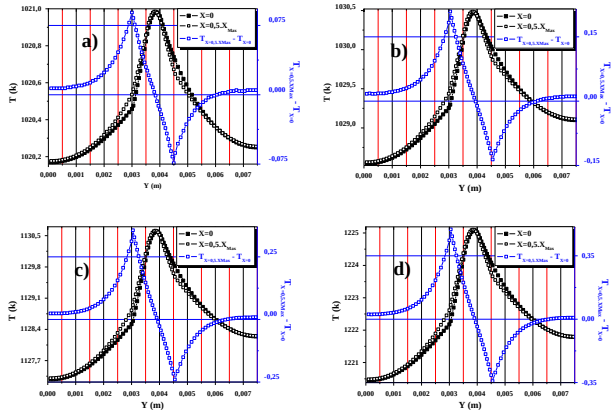

Figure 8. Temperature evolution on the (OZ) axis at (x = 0 and x = 0.5.x$_{max}$) at the cell outlet according to the current density. a) 4000 A/m^2, b) 6000 A/m^2, c) 12000 A/m^2, d) 20000 A/m^2

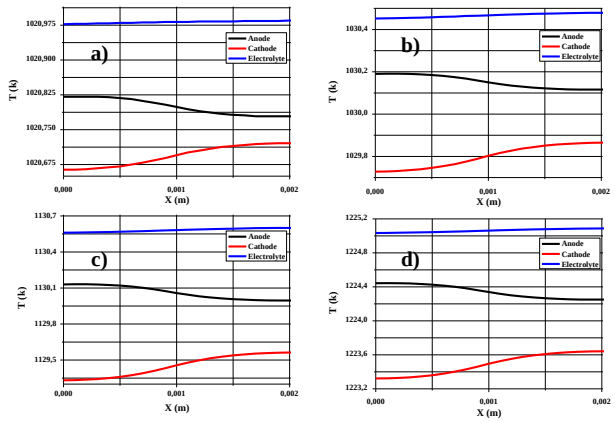

Figure 9. Temperature evolution on the (OX) axis at the cell outlet according to the current density. a) 4000 A/m^2, b) 6000 A/m^2, c) 12000 A/m^2, d) 20000 A/m^2

From Figure 9, all presented curves have almost the same reading. The electrolyte is the hottest component among all cell components, due to its ionic transport characteristic that leads to a high electrical resistivity. In addition, the anode middle is hotter than the cathode middle because of its high electrical resistance.

Figure 10 illustrates the temperature values evolution versus the current density value (4000, 6000, 12000, and 20000 A/m^2) at the position (z = 0.5.z$_{max}$ and x = 0.5.x$_{max}$) from the inlet to outlet of the cell.

At the cell having a current density value of 4000 A/m^2, the temperature decrease is clearly shown from the inlet to the cell outlet. However, there is not the same for the gases inlet temperatures that are found to remarkably increase on the (OY) axis in the cases of current density values 6000, 12000, and 20000 A/m^2 (Figure 10).

Figure 11 shows the maximum temperature evolution according to the current density in the cell.

The used scale in Figure 11 is logarithmic for the current density values and it is linear for the maximum temperature values. At the curve beginning, the maximum temperature value remains constant at a value of 1023 K (gas inlet temperature) until the joule's effect becomes important. Then, the evolution of the maximum temperature values develops with a parabolic shape according to the evolution of current density values.

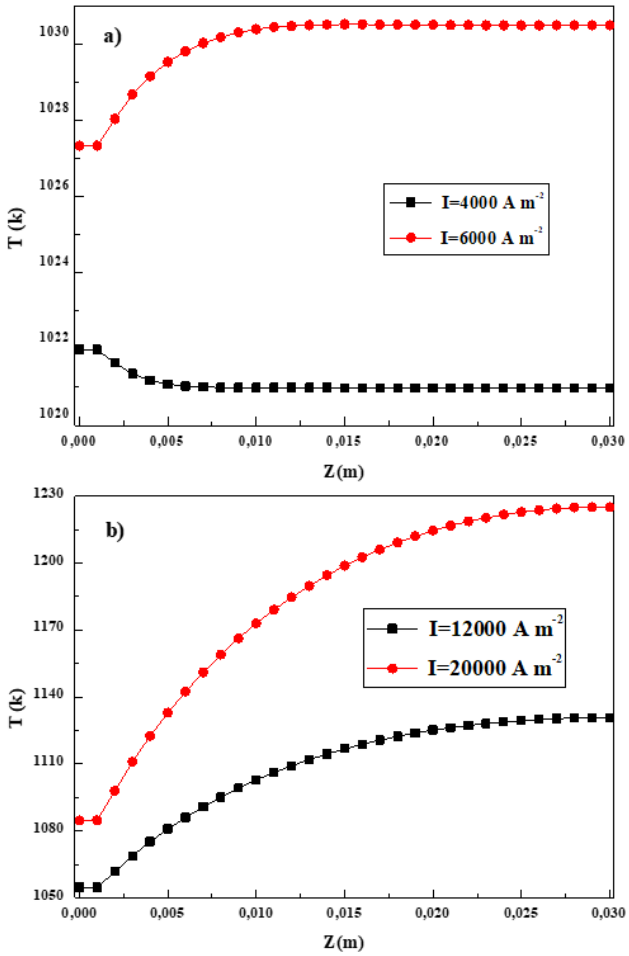

Figure 10. Temperature evolution on the (OY) axis at ($z = 0.5.z_{max}$ and $x = 0.5.x_{max}$) according to the current density value. a) 4000 and 6000 A/m^2, a) 12000 and 20000 A/m^2

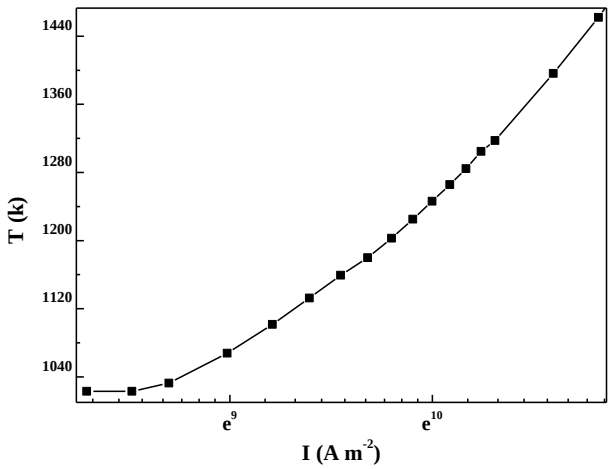

Figure 11. Maximum temperature evolution according to the current density

4. CONCLUSIONS

This investigation aims to evaluate and determine the temperature distributions within only one unit of P-SOFC at different current densities generated by the cell itself, using a steady-state three-dimensional model by considering only the Joule's effect as an internal heat source. From the obtained results' analysis, it appeared that the proposed model allowed us to assess the ohmic loss and current density effects on the overheating of the studied P-SOFC. The results reveal that the raising in the current density value entrains a raising in temperature value. The Joule's effect does not produce heat at current densities less than 5000 A/m^2. The cell upper part (anode, anodic channel and interconnect) is warmer than the cell lower part (cathode interconnector and cathodic channel) whatever the current density values and regardless of the case (heat productive or non-productive). Besides, the existence of a field symmetry to the (OZ) axis is observed at $x = 0.5.x_{max}$ position in all studied cases. The electrolyte is the hottest component due to its ionic transport characteristic that permits a high electrical resistance. The anode is hotter than the cathode, while the interconnectors are the least hot components. The electrolyte and anode centers are warmer than their wings, unlike the cathode center, which is less hot compared to its wings. Finally, as the perspectives of this work, we have interested to prepare a CFD model of the P-SOFC, which aims to study physical parameters' impact and their relationship with temperature and compare them with the present work.

REFERENCES

[1] Inui, Y., Urata, A., Ito, N., Nakajima, T., Tanaka, T. (2006). Performance simulation of planar SOFC using mixed hydrogen and carbon monoxide gases as fuel. Energy Conversion and Management, 47(13-14): 1738-1747. https://doi.org/10.1016/j.enconman.2005.10.014

[2] Sun, C.L., Ou, H.C. (2008). Numerical characterization of a microscale solid-oxide fuel cell. Journal of Power Sources, 185(1): 363-373. https://doi.org/10.1016/j.jpowsour.2008.06.048

[3] Danilov, V.A., Tade, M.O. (2009). A CFD-based model of a planar SOFC for anode flow field design. International Journal of Hydrogen Energy, 34(21): 8998-9006. https://doi.org/10.1016/j.ijhydene.2009.08.073

[4] Chaisantikulwat, A., Diaz-Goano, C., Meadows, E.S. (2008). Dynamic modelling and control of planar anode-supported solid oxide fuel cell. Computers & Chemical Engineering, 32(10): 2365-2381. https://doi.org/10.1016/j.compchemeng.2007.12.003

[5] Yang, Y., Wang, G., Zhang, H., Xia, W. (2007). Computational analysis of thermo-fluid and electrochemical characteristics of MOLB-type SOFC stacks. Journal of Power Sources, 173(1): 233-239. https://doi.org/10.1016/j.jpowsour.2007.06.070

[6] Ho, T.X., Kosinski, P., Hoffmann, A.C., Vik, A. (2009). Numerical analysis of a planar anode-supported SOFC with composite electrodes. International Journal of Hydrogen Energy, 34(8): 3488-3499. https://doi.org/10.1016/j.ijhydene.2009.02.016

[7] Khaleel, M.A., Lin, Z., Singh, P., Surdoval, W., Collin, D. (2004). A finite element analysis modeling tool for solid oxide fuel cell development: Coupled electrochemistry, thermal and flow analysis in MARC®. Journal of Power Sources, 130(1-2): 136-148. https://doi.org/10.1016/j.jpowsour.2003.11.074

[8] Wang, G., Yang, Y., Zhang, H., Xia, W. (2007). 3-D model of thermo-fluid and electrochemical for planar SOFC. Journal of Power Sources, 167(2): 398-405. https://doi.org/10.1016/j.jpowsour.2007.02.019

[9] Andreassi, L., Rubeo, G., Ubertini, S., Lunghi, P., Bove, R. (2007). Experimental and numerical analysis of a radial flow solid oxide fuel cell. International Journal of Hydrogen Energy, 32(17): 4559-4574. https://doi.org/10.1016/j.ijhydene.2007.07.047

[10] Peksen, M. (2013). 3D thermomechanical behaviour of solid oxide fuel cells operating in different environments. International Journal of Hydrogen Energy, 38(30): 13408-13418. https://doi.org/10.1016/j.ijhydene.2013.07.112

[11] Peksen, M., Peters, R., Blum, L., Stolten, D. (2009). Numerical modelling and experimental validation of a planar type pre-reformer in SOFC technology. International Journal of Hydrogen Energy, 34(15): 6425-6436. https://doi.org/10.1016/j.ijhydene.2009.06.017

[12] Peksen, M., Al-Masri, A., Blum, L., Stolten, D. (2013). 3D transient thermomechanical behaviour of a full scale SOFC short stack. International Journal of Hydrogen Energy, 38(10): 4099-4107. https://doi.org/10.1016/j.ijhydene.2013.01.072

[13] Nakajo, A., Mueller, F., Brouwer, J., Favrat, D. (2012). Mechanical reliability and durability of SOFC stacks. Part I: Modelling of the effect of operating conditions and design alternatives on the reliability. International Journal of Hydrogen Energy, 37(11): 9249-9268. https://doi.org/10.1016/j.ijhydene.2012.03.043

[14] Nakajo, A., Mueller, F., Brouwer, J., Favrat, D. (2012). Mechanical reliability and durability of SOFC stacks. Part II: Modelling of mechanical failures during ageing and cycling. International Journal of Hydrogen Energy, 37(11): 9269-9286. https://doi.org/10.1016/j.ijhydene.2012.03.023

[15] Jiang, T.L., Chen, M.H. (2009). Thermal-stress analyses of an operating planar solid oxide fuel cell with the bonded compliant seal design. International Journal of Hydrogen Energy, 34(19): 8223-8234. https://doi.org/10.1016/j.ijhydene.2009.07.089

[16] Hawkes, G., O'Brien, J., Stoots, C., Hawkes, B. (2009). 3D CFD model of a multi-cell high-temperature electrolysis stack. International Journal of Hydrogen Energy, 34(9): 4189-4197. https://doi.org/10.1016/j.ijhydene.2008.11.068

[17] Lee, S.F., Hong, C.W. (2010). Multi-scale design simulation of a novel intermediate-temperature micro solid oxide fuel cell stack system. International Journal of Hydrogen Energy, 35(3): 1330-1338. https://doi.org/10.1016/j.ijhydene.2009.11.095

[18] Yan, D., Bin, Z., Fang, D., Luo, J., Wang, X., Pu, J., Zhang, Y. (2013). Feasibility study of an external manifold for planar intermediate-temperature solid oxide fuel cells stack. International Journal of Hydrogen Energy, 38(1): 660-666. https://doi.org/10.1016/j.ijhydene.2012.06.020

[19] Youcef, S., Bariza, Z., Houcine, M., Hocine, B.M. (2019). Three-dimensional numerical study of the anode supported intermediate temperature solid oxide fuel cell overheating. International Journal of Heat and Technology, 37(4): 1099-1106. https://doi.org/10.18280/ijht.370419

[20] Hohammedi, A., Ben moussa, H., Tamerabet, M., Sahli, Y. (2020). Numerical investigation of the effects of channel cross section shape on the tubular PEMFC performance. Journal of Advanced Research in Fluid Mechanics and Thermal Sciences, 66(1): 84-103.

[21] Sahli, Y. (2022). Thermodynamic modeling and analysis of proton ceramic fuel cells: Power optimization. Arabian Journal for Science and Engineering, 47(5): 6355-6363. https://doi.org/10.1007/s13369-021-06262-7

[22] Sahli, Y., Zitouni, B., Benmoussa, H. (2018). Etude numérique tridimensionnelle de l'effet de la température d'entrée des gaz sur la production de chaleur dans une pile à combustible SOFC planaire. Journal of Renewable Energies, 21(2): 173-180.

[23] Mohammedi, A., Sahli, Y., Moussa, H.B. (2020). Optimization study of the produced electric power by planar PEMFC-SCG. Renewable Energy Focus, 35: 72-83. https://doi.org/10.1016/j.ref.2020.09.003

[24] Laribi, S., Mammar, K., Sahli, Y., Necaibia, A., Arama, F.Z., Ghaitaoui, T. (2021). PEMFC water diagnosis using PWM functionality signal and fractional order model. Energy Reports, 7: 4214-4221. https://doi.org/10.1016/j.egyr.2021.07.010

[25] Sahli, Y., Moussa, H.B., Zitouni, B. (2019). Optimization study of the produced electric power by SOFCs. International Journal of Hydrogen Energy, 44(39): 22445-22454. https://doi.org/10.1007/978-981-15-6595-3_26.

[26] Sahli, Y., Zitouni, B., Hocine, B.M. (2021). Three-dimensional numerical study of overheating of two intermediate temperature P-AS-SOFC geometrical configurations. In Hydrogen Fuel Cell Technology for Stationary Applications, 186-222. https://doi.org/10.4018/978-1-7998-4945-2.ch008

[27] Abdenebi, H., Zitouni, B., Ben Moussa, H., Haddad, D., Zitouni, H., Sahli, Y. (2015). Inlet methane temperature effect at a planar SOFC thermal field under direct internal reforming condition. In Progress in Clean Energy, 2: 567-581. https://doi.org/10.1007/978-3-319-17031-2_41

[28] Sahli, Y., Zitouni, B., Ben Moussa, H., Abdenebi, H. (2015). Three-dimensional numerical study of the heat transfer on the planar solid oxide fuel cell: Joules effect. In Progress in Clean Energy, 1: 449-461. https://doi.org/10.1007/978-3-319-16709-1_32

[29] Sahli, Y., Zitouni, B., Ben-Moussa, H. (2018). Thermodynamic optimization of the solid oxyde fuel cell electric power. University Politehnica of Bucharest Scientific Bulletin Series B-Chemistry and Materials Science, 80(2): 159-170.

[30] Sahli, Y., Moussa, H.B., Zitouni, B. (2019). Optimization study of the produced electric power by SOFCs. International Journal of Hydrogen Energy, 44(39): 22445-22454. https://doi.org/10.1016/j.ijhydene.2018.08.162

[31] Sahli, Y., Zitouni, B., Hocine, B.M. (2017). Solid oxide fuel cell thermodynamic study. Çankaya University Journal of Science and Engineering, 14(2): 134-151.

[32] Aguiar, P., Adjiman, C.S., Brandon, N.P. (2004). Anode-supported intermediate temperature direct internal reforming solid oxide fuel cell. I: Model-based steady-state performance. Journal of Power Sources, 138(1-2): 120-136. https://doi.org/10.1016/j.jpowsour.2004.06.040

[33] Ferguson, J.R., Fiard, J.M., Herbin, R. (1996). Three-dimensional numerical simulation for various geometries of solid oxide fuel cells. Journal of Power Sources, 58(2): 109-122. https://doi.org/10.1016/0378-7753(95)02269-4

[34] Hussain, M.M., Li, X., Dincer, I. (2006). Mathematical modeling of planar solid oxide fuel cells. Journal of

Power Sources, 161(2): 1012-1022. https://doi.org/10.1016/j.jpowsour.2006.05.055
[35] Zhang, X., Li, G., Li, J., Feng, Z. (2007). Numerical study on electric characteristics of solid oxide fuel cells. Energy Conversion and Management, 48(3): 977-989. https://doi.org/10.1016/j.enconman.2006.08.011
[36] Zinovik, I., Poulikakos, D. (2009). Modeling the temperature field in the reforming anode of a button-shaped solid oxide fuel cell. Electrochimica Acta, 54(26): 6234-6243. https://doi.org/10.1016/j.electacta.2009.06.001
[37] Bao, C., Cai, N., Croiset, E. (2011). A multi-level simulation platform of natural gas internal reforming solid oxide fuel cell–gas turbine hybrid generation system–Part II. Balancing units model library and system simulation. Journal of Power Sources, 196(20): 8424-8434. https://doi.org/10.1016/j.jpowsour.2011.05.032
[38] Verma, J.K., Verma, A., Ghoshal, A.K. (2013). Performance analysis of solid oxide fuel cell using reformed fuel. International Journal of Hydrogen Energy, 38(22): 9511-9518. https://doi.org/10.1016/j.ijhydene.2013.01.158
[39] Andersson, M., Yuan, J., Sundén, B. (2013). SOFC modeling considering hydrogen and carbon monoxide as electrochemical reactants. Journal of Power Sources, 232: 42-54. https://doi.org/10.1016/j.jpowsour.2012.12.122
[40] Andersson, M., Paradis, H., Yuan, J., Sundén, B. (2013). Three dimensional modeling of an solid oxide fuel cell coupling charge transfer phenomena with transport processes and heat generation. Electrochimica Acta, 109: 881-893. https://doi.org/10.1016/j.electacta.2013.08.018
[41] Ni, M., Leung, M.K., Leung, D.Y. (2007). Parametric study of solid oxide fuel cell performance. Energy Conversion and Management, 48(5): 1525-1535. https://doi.org/10.1016/j.enconman.2006.11.016
[42] Chyou, Y.P., Chung, T.D., Chen, J.S., Shie, R.F. (2005). Integrated thermal engineering analyses with heat transfer at periphery of planar solid oxide fuel cell. Journal of Power Sources, 139(1-2): 126-140. https://doi.org/10.1016/j.jpowsour.2004.07.001
[43] Ramakrishna, P.A., Yang, S., Sohn, C.H. (2006). Innovative design to improve the power density of a solid oxide fuel cell. Journal of Power Sources, 158(1): 378-384. https://doi.org/10.1016/j.jpowsour.2005.10.030
[44] Damm, D.L., Fedorov, A.G. (2006). Reduced-order transient thermal modeling for SOFC heating and cooling. Journal of Power Sources, 159(2): 956-967. https://doi.org/10.1016/j.jpowsour.2005.11.072
[45] Mahcene, H., Moussa, H.B., Bouguettaia, H., Bechki, D., Babay, S., Meftah, M.S. (2011). Study of species, temperature distributions and the solid oxide fuel cells performance in a 2-D model. International Journal of Hydrogen Energy, 36(6): 4244-4252. https://doi.org/10.1016/j.ijhydene.2010.07.075
[46] Ota, T., Koyama, M., Wen, C.J., Yamada, K., Takahashi, H. (2003). Object-based modeling of SOFC system: Dynamic behavior of micro-tube SOFC. Journal of Power Sources, 118(1-2): 430-439. https://doi.org/10.1016/S0378-7753(03)00109-5
[47] Petruzzi, L., Cocchi, S., Fineschi, F. (2003). A global thermo-electrochemical model for SOFC systems design and engineering. Journal of Power Sources, 118(1-2): 96-107. https://doi.org/10.1016/S0378-7753(03)00067-3
[48] Suwanwarangkul, R., Croiset, E., Pritzker, M.D., Fowler, M.W., Douglas, P.L., Entchev, E. (2006). Mechanistic modelling of a cathode-supported tubular solid oxide fuel cell. Journal of Power Sources, 154(1): 74-85. https://doi.org/10.1016/j.jpowsour.2005.03.197
[49] Kakac, S., Pramuanjaroenkij, A., Zhou, X.Y. (2007). A review of numerical modeling of solid oxide fuel cells. International Journal of Hydrogen Energy, 32(7): 761-786. https://doi.org/10.1016/j.ijhydene.2006.11.028
[50] Sangtongkitcharoen, W., Vivanpatarakij, S., Laosiripojana, N., Arpornwichanop, A., Assabumrungrat, S. (2008). Performance analysis of methanol-fueled solid oxide fuel cell system incorporated with palladium membrane reactor. Chemical Engineering Journal, 138(1-3): 436-441. https://doi.org/10.1016/j.cej.2007.06.021